Two-dimensional hydrodynamic flow focusing in a microfluidic platform featuring a monolithic integrated glass micronozzle

Yifan Liu, Yusheng Shen, Lian Duan, and Levent Yobas

Articles you may be interested in

Microfluidic emulsification through a monolithic integrated glass micronozzle suspended inside a flow-focusing geometry
Appl. Phys. Lett. **106**, 174101 (2015); 10.1063/1.4919444

Two- and three-dimensional modeling and optimization applied to the design of a fast hydrodynamic focusing microfluidic mixer for protein folding
Phys. Fluids **25**, 032001 (2013); 10.1063/1.4793612

Production rate and diameter analysis of spherical monodisperse microbubbles from two-dimensional, expanding-nozzle flow-focusing microfluidic devices
Biomicrofluidics **7**, 014103 (2013); 10.1063/1.4774069

An integrated, multiparametric flow cytometry chip using "microfluidic drifting" based three-dimensional hydrodynamic focusing
Biomicrofluidics **6**, 024113 (2012); 10.1063/1.3701566

Three-dimensional hydrodynamic focusing in a microfluidic Coulter counter
Rev. Sci. Instrum. **79**, 046104 (2008); 10.1063/1.2900010

Two-dimensional hydrodynamic flow focusing in a microfluidic platform featuring a monolithic integrated glass micronozzle

Yifan Liu,[1] Yusheng Shen,[1,2] Lian Duan,[1] and Levent Yobas[1,2,a]

[1]*Department of Electronic and Computer Engineering, Hong Kong University of Science and Technology, Hong Kong, People's Republic of China*
[2]*Division of Biomedical Engineering, Hong Kong University of Science and Technology, Hong Kong, People's Republic of China*

Two-dimensional hydrodynamic flow focusing is demonstrated through a microfluidic device featuring a monolithic integrated glass micronozzle inside a flow-focusing geometry. Such a coaxial configuration allows simple one-step focusing of a sample fluid stream, jetted from the micronozzle tip, in both in-plane and out-of-plane directions. The width of the focused filament can be precisely controlled and further scaled down to the submicrometer regime to facilitate rapid hydrodynamic mixing. Fluorescence quenching experiments reveal ultra-fast microsecond mixing of the denaturant into the focused filament. This device offers new possibilities to a set of applications such as the study of protein folding kinetics. *Published by AIP Publishing.*
[http://dx.doi.org/10.1063/1.4964263]

The advance of microfluidic techniques has shown great capability in precisely manipulating fluids and particles.[1] Hydrodynamic flow focusing, for instance, enables the compression of a fluid stream by coflowing the sheath flows in a microchannel, which has been broadly used in the fields of chemical and biological analysis, including on-chip flow cytometry,[2,3] chemical synthesis,[4] and microsecond hydrodynamic mixers for the study of protein kinetics.[5,6] For most of such applications, focusing the center flow in both horizontal and vertical directions is highly desired, yet the planar nature of microfluidic devices fabricated via standard lithographic techniques facilitates well-controlled focusing only in the in-plane (horizontal) direction. This has led to practical issues such as vertical spread of cells in on-chip flow cytometry[7] and non-uniformity of the mix time along the channel depth in hydrodynamic mixers.[6,8]

Two-dimensional (2D) hydrodynamic focusing can be realized by using an axial-symmetric flow focusing geometry, which is conventionally formed through the coaxial assembly of glass capillaries.[9,10] However, the robustness and manufacturability of the system are remaining concerns that may hinder its widespread use. Monolithic integration of similar coaxial flow geometry on a microfluidic chip that can be conveniently fabricated via standard lithographic techniques can potentially address such concerns, yet implementing such configuration is challenging due to difficulties in the fabrication of a suspended micronozzle and its microfluidic integration as a coaxial flow geometry. Therefore, considerable effort has been devoted to innovative 2D focusing strategies that can be easily realized on a planar microfluidic device. A representative strategy is focusing the target fluid in horizontal and vertical directions separately at distinctive flow-focusing junctions.[11] However, this method requires increased number of flow injection pumps and laborious optimization of the flow rates to focus the target stream in

the center of the microchannel. Moreover, flow focusing in the out-of-plane direction is less controllable due to the planar configuration of the vertical focusing geometry. Mao *et al.* presented an ingenious approach of 2D hydrodynamic focusing, which took advantage of a transverse secondary flow induced by the centrifugal effect in a curved microchannel to laterally drift the sample stream,[3,12] but this approach is not suitable for important applications such as rapid hydrodynamic mixing which requires extremely high flow velocity (in the order of 1 m/s) and extremely narrow (sub-micrometer) focused streams.[13]

In this paper, we present an integrated microfluidic device for well-defined and controllable 2D hydrodynamic focusing. Fig. 1 schematically illustrates the device structure in which a single suspended micronozzle is integrated inside a flow-focusing geometry. The sample fluid is supplied through a buried channel at the opposing end and ejected at the tip of the micronozzle into the coflowing stream of the sheath flow. Such configuration allows similar mechanism as of the coaxial flow-focusing geometry (the concentric assembly of glass capillaries)[10] and thus enables a fine focusing of the sample flow in both in-plane and out-of-plane directions. The suspended micronozzle is a released segment of a self-enclosed microchannel featuring a cylindrical lumen that is evolved from a void trapped inside a partially-filled silicon trench.[14] Therefore, the entire fabrication process is compatible with standard semiconductor manufacturing techniques.

The device fabrication process is briefly described through the illustrations in Fig. 2. The fabrication was initiated with the deposition of a phosphosilicate glass (PSG) layer, 5 μm thick, on silicon having a trench, 3 μm wide and deep, created by deep reactive ion etch (DRIE), Figs. 2(a) and 2(b). The non-conformal step coverage by the deposited glass layer led to a self-enclosed void elongated within the trench. The void was subsequently allowed to undergo shape transformation into a cylindrical tube *via* glass reflow driven by the surface tension forces during a thermal anneal step in N$_2$ ambient (1000 °C for 1 h), Fig. 2(c). A detailed parametric study of the

a)Author to whom correspondence should be addressed. Electronic mail: eelyobas@ust.hk
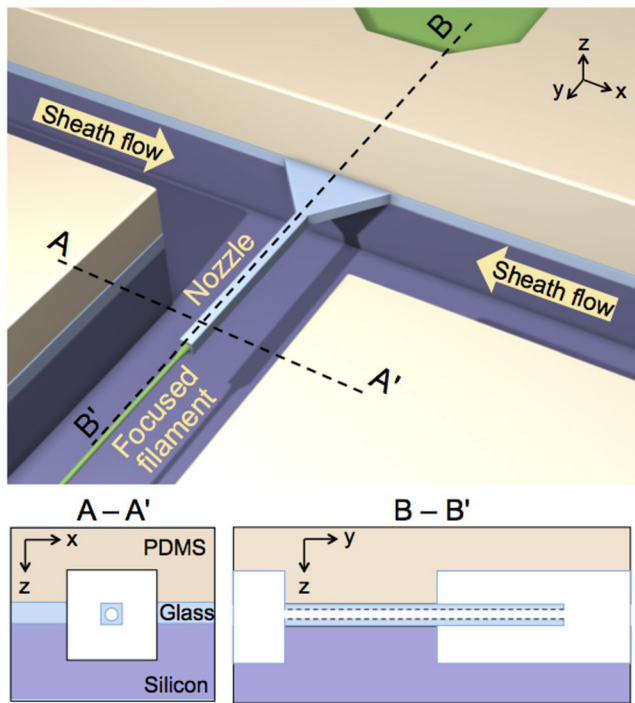
FIG. 1. 3D rendering of the microfluidic device. The device features a single suspended micronozzle integrated inside a conventional flow-focusing geometry. The micronozzle is entirely defined in a glass layer situated between a silicon substrate and a PDMS cover plate. The lower panel shows $x - z$ (along A–A$'$) and $y - z$ (along B–B$'$) cross-sections of the flow-focusing junction.

cylindrical glass capillary formation was previously presented elsewhere.[14] The monolithic integration of the as-formed cylindrical tube into the flow-focusing geometry was realized *via* standard photolithographic techniques and subsequent dry etching steps. First, the glass layer was exposed and removed through a resist mask by advanced oxide etch (AOE),
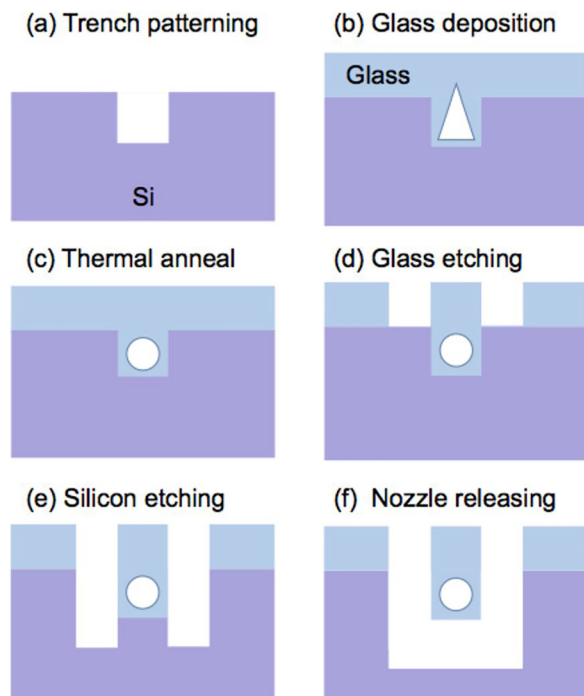
FIG. 2. Description of the device fabrication process through the illustrations of the device substrate ($x - z$ cross-section) after key fabrication steps (not drawn to scale).

Fig. 2(d). The underlying silicon was subsequently etched to a depth of $30\,\mu m$ by DRIE, Fig. 2(e). These steps defined the flow focusing geometry and outlined the segment of the buried cylindrical tube that would be released into a suspended micronozzle. The release step was performed through an isotropic dry etch in SF_6 plasma for about 3 min and led to a nominal final depth of $40\,\mu m$, Fig. 2(f).

Fig. 3 displays scanning electron micrographs of the flow-focusing geometry taken from a representative device in various perspectives. The suspended micronozzle features a length of $200\,\mu m$ and a circular opening of $1.5\,\mu m$ in diameter, Fig. 3(b). Before the experiments, a polydimethylsiloxane (PDMS) slab was secured on the fabricated chip through oxygen plasma activation to form the inlet/outlet ports. The PDMS slab was patterned with the same flow-focusing layout ($40\,\mu m$ in height) through standard soft lithography and carefully aligned to the chip in order to situate the suspended micronozzle in the center of the focusing geometry (Fig. 1, lower panel). In the experiments, the sample and sheath flows were delivered into respective channels using syringe pumps (Harvard apparatus, S. Natick, MA). The flow directions at the focusing junction are denoted in Fig. 3(c).

To evaluate the flow-focusing behavior in our device, we labeled the sample stream with fluorescein isothiocyanate-dextran (FITC-dextran, Sigma-Aldrich, St. Louis, MO) and inspected the focused sample stream under a confocal scanning microscope (Zeiss LSM 7 DUO, Carl Zeiss MicroImaging GmbH, Jena, Germany). In order to minimize the diffusion of fluorescent molecules into the sheath flow, high molecular weight ($MW \sim 2\,000\,000$) FITC-dextran was used. The molecules were spiked in 100 mM KCl to a final concentration $6\,\mu M$ as the sample fluid, whereas the sheath fluid was 100 mM KCl solution. Fig. 4(a) depicts laser scanning micrographs of the focused sample stream obtained at various outer sheath flow rates (Q_{out}), whereas the inner sample flow rate (Q_{in}) was kept constant, $0.02\,\mu l/min$, throughout the experiment. Also note that the laser intensity was increased when imaging the focusing event at $Q_{out} = 0.2\,ml/min$ to better
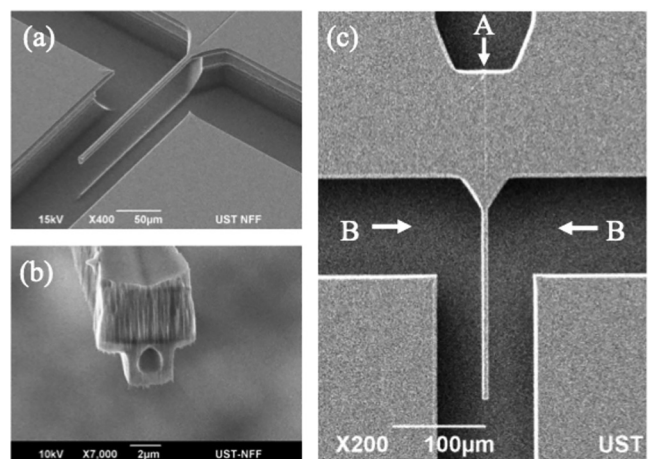
FIG. 3. Scanning electron micrographs: (a) isometric view of the flow-focusing geometry depicting the single suspended glass micronozzle integrated on silicon, (b) close-up view of the micronozzle tip revealing the circular opening, and (c) planar view of the microfluidic design with the arrows denoting the flow directions labeled as (A) for the sample flow and (B) for the sheath flows.
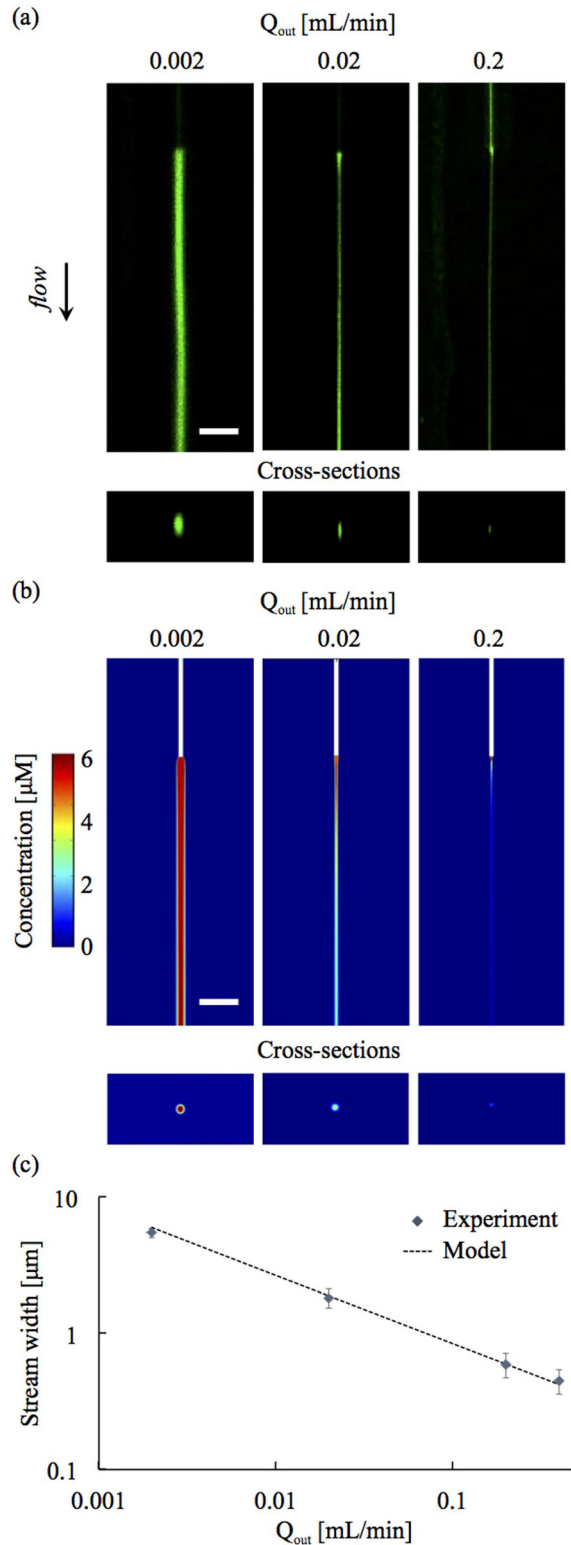
FIG. 4. Two-dimensional hydrodynamic focusing in the microfluidic device. (a) Confocal micrographs and (b) corresponding simulation results of the focused center stream (FITC-dextran; $Q_{in} = 0.02$ μl/min) at a set of distinct outer flow rates, Q_{out}. (c) The focused stream width plotted as a function of the outer flow rate. The dashed line is described by Eq. (7). Scale bars: 20 μm. The excitation laser (489 nm) power was set to 1.5, 4.25, and 6.5 mW when imaging the focused stream at Q_{out} set to 0.002, 0.02, and 0.2 ml/min, respectively.

visualize the focused stream. As shown, the sample fluid formed a well-defined thin filament in the coflowing stream of the sheath flow; when Q_{out} was increased from 0.002 to 0.2 ml/min, the focused filament was further narrowed while

maintaining its uniformity in width. The cross-sectional images reveal a quasi-circular profile of the focused filament, which clearly suggests a fine 2D hydrodynamic focusing behavior in our device. To further validate the focusing, we simulated the three-dimensional laminar flow and diffusion dynamics in the flow focusing geometry. The numerical simulation was performed in COMSOL Multiphysics Software v4.3 (Comsol Inc., Burlington, MA) based on the incompressible steady-state Navier-Stokes equations and the steady-state convective-diffusion equation

$$\nabla \cdot \vec{V} = 0, \tag{1}$$

$$\rho(\vec{V} \cdot \nabla)\vec{V} = -\nabla P + \mu \nabla^2 \vec{V}, \tag{2}$$

$$\vec{V} \cdot \nabla C = D \nabla^2 C, \tag{3}$$

where $\vec{V}$ denotes the flow velocity, ρ the fluid density, P the pressure, μ the fluid dynamic viscosity, C the concentration of FITC-dextran, and D the diffusivity of FITC-dextran in water. To allow direct comparison of the simulated and experimental results, the boundary conditions (Q_{in}, Q_{out}) in the simulation were set identical to those of the experiments. As shown in Fig. 4(b), the simulation also revealed a 2D focused thin filament featuring a circular cross-section, which is in strong agreement with the experimental results in Fig. 4(a). Such results verify that our device is capable of performing fine 2D flow focusing.

To further characterize the flow-focusing behavior, we developed a model that describes the relation between the width of the achieved filaments and input flow rates. The model is based on the approximation that the focused filament has a circular profile and a uniform velocity across its width. Using the relation

$$Q_{in} = V_f \cdot \pi r^2, \tag{4}$$

where V_f and r denote the steady-state flow velocity and cross-sectional radius of the focused filament, respectively, and the width of the focused filament w can be derived as

$$w = 2r = 2\sqrt{\frac{Q_{in}}{\pi V_f}}. \tag{5}$$

As the micronozzle is centered in the rectangular collecting channel, V_f is the maximum velocity of the pressure driven flow, given as

$$V_f = \frac{3}{2} \cdot \frac{Q}{WH}, \tag{6}$$

where W and H denote the width and height of the collecting channel, respectively, and $Q = Q_{in} + Q_{out}$ the total volumetric flow rate in the channel. Given that $Q_{in} \ll Q_{out}$, combining Eqs. (5) and (6), w can be expressed as

$$w = \sqrt{\frac{8}{3\pi}} \cdot \sqrt{WH \cdot \frac{Q_{in}}{Q_{out}}}. \tag{7}$$

As Q_{in} was kept constant in our experiments, w is solely dependent on Q_{out}. Therefore, we plotted w as a function of

Q_{out} in comparison to experimentally obtained w values in Fig. 4(c). As shown, the experimental values are in close agreement with the theoretical predictions, which validates that the model is capable of accurately describing the flow-focusing characteristic in our device.

An essential application of hydrodynamic focusing devices is performing rapid mixing for protein folding studies.[5,13] To investigate whether our device can be potentially used in such studies, we performed FITC-dextran quenching experiments to evaluate its mixing characteristics. The experiments were conducted at a higher outer flow rate, 0.4 ml/min, whereas Q_{in} was kept as previously stated. Under this particular condition, the focused filament features a width of $\sim$420 nm and a steady-state velocity of $\sim$1.2 m/s. The quenching of FITC-dextran was realized by replacing the outer fluid to 0.5 M potassium iodide (KI). To quantify the quenching process, we imaged the focused FITC-dextran filament before and after the quenching, and defined the quenched intensity ratio (R): $R = I(q)/I(uq)$, where $I(q)$ and $I(uq)$ are the quenched and unquenched fluorescent intensities of the FITC-dextran filament, respectively. We obtained R at single pixel resolution along the filament centerline and plotted R as a function of traveling distance (x) by converting pixel numbers to spatial coordinates. As shown in Fig. 5(a), R was decreased drastically when FITC-dextran molecules were released from the micronozzle tip ($x > 0$), and reached a plateau after a traveling distance of 20 μm. This result
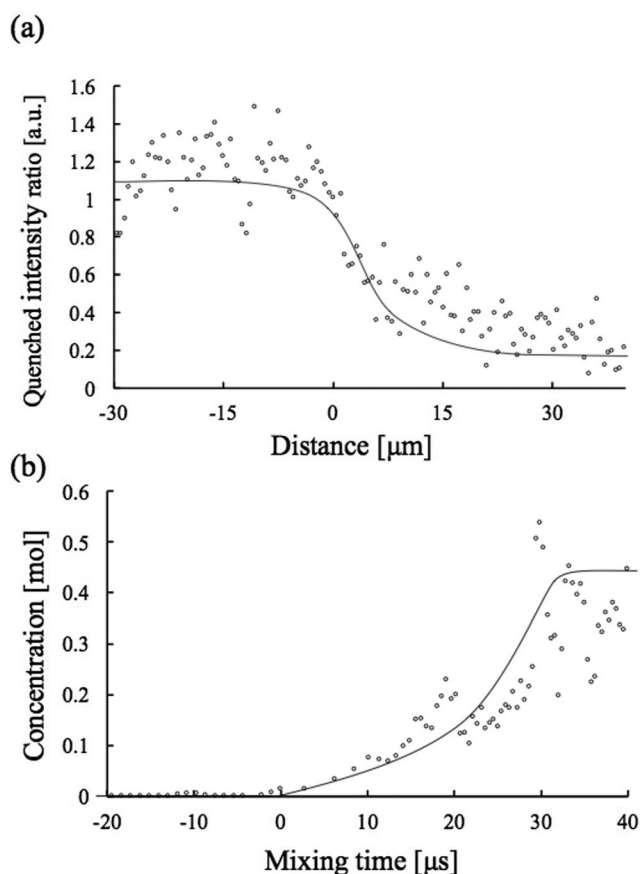
confirms the occurrence of quenching as a result of fast mixing of KI with FITC-dextran. To estimate the characteristic mixing time of the experiment, we integrated the function $1/V(x)$ along the focused stream centerline using the numerical velocity field obtained by the simulation, which converted the spatial coordinate, x, to a Lagrangian time coordinate, t. In addition, we converted the ratio R to KI concentration by off-chip calibration of FITC-dextran quenching in KI solution. Fig. 5(b) displays the obtained KI concentration *versus* mixing time, where the characteristic mixing time can be estimated to be $\sim$30 μs. Such a performance is satisfactory for applications such as protein folding studies which require fast mixing in less than 100 μs.[15]

A key feature of the introduced design is that the fluid upon emerging from the micronozzle tip is readily focused into a fine jet. Thus, the time delay between the onset of diffusional mixing and the complete focusing is greatly reduced in comparison to delays encountered in conventional hydrodynamic micromixers. In conventional hydrodynamic micromixers, the delay could be significant and the resultant "premixing" (premature mixing prior to the formation of a focused jet) introduces large uncertainties in the mix time evaluation. The premixing can be reduced by increasing the flow rate but at the expense of increased sample consumption. The issue can be alternatively addressed by adopting a five-inlet-port junction that incorporates a barrier sheath flow in between the streams to be mixed. Yet, the mix time evaluation in such design remains sensitive to operating conditions.[16] The premixing issue has also motivated micromixer designs with the focused stream inlet at an ever-shrinking channel width.[17] Apart from shrinking the focused stream inlet below 2 μm, the integrated micronozzle demonstrated in this study keeps the focused stream away from the top and bottom channel walls, ensuring a more uniform velocity profile for the focused stream and allowing for a more accurate determination of the mix time.

In conclusion, we have demonstrated an integrated and robust microfluidic platform for well-defined two-dimensional flow focusing. The focusing is achieved by a suspended glass micronozzle integrated inside a flow-focusing geometry where a thin filament of the sample fluid can be directly injected from the tip of the micronozzle into the coflowing sheath fluid. With the feature of a microsecond fast mixing, the device can be potentially used in the study of protein folding kinetics and other fast-occurring nonequilibrium biochemical processes. The mixing time can be further reduced by narrowing the collecting microchannel and hence increasing the flow velocity. Current effort is underway to optimize the microfluidic design for achieving uniform mixing in less than 10 μs.

FIG. 5. FITC-dextran quenching experiments. (a) Quenched intensity ratio as a function of traveling distance. (b) Potassium iodide concentration as a function of the mixing time. Experimental condition: Q_{out} = 0.4 ml/min; Q_{in} = 0.02 μl/min; focused stream width $\sim$420 nm.

[1]T. M. Squires and S. R. Quake, Rev. Mod. Phys. **77**, 977 (2005).
[2]M. M. Wang, E. Tu, D. E. Raymond, J. M. Yang, H. C. Zhang, N. Hagen, B. Dees, E. M. Mercer, A. H. Forster, I. Kariv, P. J. Marchand, and W. F. Butler, Nat. Biotechnol. **23**, 83 (2005).
[3]X. L. Mao, S. C. S. Lin, C. Dong, and T. J. Huang, Lab Chip **9**, 1583 (2009).
[4]R. R. Hood, D. L. DeVoe, J. Atencia, W. N. Vreeland, and D. M. Omiatek, Lab Chip **14**, 2403 (2014).
[5]J. B. Knight, A. Vishwanath, J. P. Brody, and R. H. Austin, Phys. Rev. Lett. **80**, 3863 (1998).

[6]L. Pollack, M. W. Tate, N. C. Darnton, J. B. Knight, S. M. Gruner, W. A. Eaton, and R. H. Austin, Proc. Natl. Acad. Sci. U S A **96**, 10115 (1999).

[7]A. Wolff, I. R. Perch-Nielsen, U. D. Larsen, P. Friis, G. Goranovic, C. R. Poulsen, J. P. Kutter, and P. Telleman, Lab Chip **3**, 22 (2003).

[8]D. E. Hertzog, B. Ivorra, B. Mohammadi, O. Bakajin, and J. G. Santiago, Anal. Chem. **78**, 4299 (2006).

[9]S. Takeuchi, P. Garstecki, D. B. Weibel, and G. M. Whitesides, Adv. Mater. **17**, 1067 (2005).

[10]A. S. Utada, E. Lorenceau, D. R. Link, P. D. Kaplan, H. A. Stone, and D. A. Weitz, Science **308**, 537 (2005).

[11]C. Simonnet and A. Groisman, Appl. Phys. Lett. **87**, 114104 (2005).

[12]X. L. Mao, J. R. Waldeisen, and T. J. Huang, Lab Chip **7**, 1260 (2007).

[13]L. G. Jiang, Y. Zeng, Q. Q. Sun, Y. R. Sun, Z. H. Guo, J. N. Y. Qu, and S. H. A. Yao, Anal. Chem. **87**, 5589 (2015).

[14]Y. F. Liu and L. Yobas, Biomicrofluidics **6**, 046502 (2012).

[15]Y. Duan and P. A. Kollman, Science **282**, 740 (1998).

[16]H. Y. Park, X. Qiu, E. Rhoades, J. Korlach, L. W. Kwok, W. R. Zipfel, W. W. Webb, and L. Pollack, Anal. Chem. **78**, 4465 (2006).

[17]D. E. Hertzog, X. Michalet, M. Jager, X. Kong, J. G. Santiago, S. Weiss, and O. Bakajin, Anal. Chem. **76**, 7169 (2004).